



Supercritical CO₂-assisted microfluidization as ultra-high efficiency strategy for graphene preparation

Nan Zhang^{1,2,3}, Yaoming Zhang¹, Chunjian Duan^{1,2,3}, Song Li^{1,2,3}, Zenghui Yang¹,
Xinrui Zhang¹, Tingmei Wang^{1,2,*}, and Qihua Wang^{1,2,3,*} 

¹Key Laboratory of Science and Technology On Wear and Protection of Materials, Lanzhou Institute of Chemical Physics, Chinese Academy of Sciences, Lanzhou 730000, China

²Center of Materials Science and Optoelectronics Engineering, University of Chinese Academy of Sciences, Beijing 100049, China

³State Key Laboratory of Solid Lubrication, Lanzhou Institute of Chemical Physics, Chinese Academy of Sciences, Lanzhou 730000, China

Received: 27 November 2020

Accepted: 4 February 2021

Published online:

13 July 2021

© The Author(s), under exclusive licence to Springer Science+Business Media, LLC, part of Springer Nature 2021

ABSTRACT

Traditional “top-down” methods for graphene preparation, like micromechanical cleavage and ultrasound methods, usually cannot preserve both efficiency and quality simultaneously. Herein, we provide an environmental-friendly graphene exfoliating method with high efficiency and high quality that combines the microfluidization process (liquid phase) and supercritical carbon dioxide process (gas phase), namely the dual-phase exfoliating (DPE) method. The combination of effective tangential force (shearing force) and normal force (push and pull), which are originally from microfluidization and supercritical carbon dioxide process, respectively, maximizes the exfoliating efficiency. The DPE method offers a high yield of up to 70.25% for graphene preparation (941.04 g per day theoretically), while the graphene sheets could remain single or a few layers (> 80%) and around micron size. By molecular dynamic simulations, it is theoretically proved that carbon dioxide can intercalate between graphite layers and expand the interlayer spacing under supercritical conditions. This DPE method, by combining the advantages of different phase processes, provides an ideal process design perspective for large-scale preparation of other 2D materials.

Handling Editor: Dale Huber.

Address correspondence to E-mail: wangqh@licp.cas.cn

<https://doi.org/10.1007/s10853-021-05903-4>

Introduction

Graphene, a single layer of carbon atoms with hexagonal lattice, has been considered as the ideal candidate for many applications owing to the enticing properties, like super mechanical strength [1], high thermal conductivity [2], high surface area [3] and the quantum mechanical effect [4]. The properties of graphene strongly depend on its size and thickness [5]. The arising demand of high-performance graphene has led to multitudinous research efforts on quality-controllable graphene preparation with cost-effective and scalable manufacturing.

It is well known that there are two strategies for graphene preparation, bottom-up and top-down method. (a) The bottom-up method is mostly based on chemical vapor deposition (CVD), by which carbon-containing molecules were used as precursors or sources to deposit on a substrate and form graphene films. However, extremely high cost and harsh preparation conditions, such as preparation and transfer of substrates, limit the industrialization; (b) top-down methods, such as micromechanical cleavage, chemical exfoliation and liquid-phase exfoliation, by which bulk graphite is separated directly into single or few layers by external forces. Chemical exfoliation and liquid-phase exfoliation [6] could overcome interlayer interactions, and they are considered as the promise methods for the industrial preparation of graphene. Due to extremely mild and easily up-scalable, liquid-phase exfoliation has been considered as an ideal strategy for graphene preparation [7]. Paton et al. developed a simple model, in which exfoliation occurs when shear rate exceeds 10^4 s^{-1} [8]; then, various devices with a high shear rate have been developed to reach the critical point, from industrial [9] to domestic mixing types of equipment [10]. However, the time-wasting (up to ten hours) and energy-consuming [11] process is uneconomic, let alone the problem of uncontrollable quality in size and thickness or the low yields.

Microfluidization is a liquid-phase method that pushes the high-pressure fluid (up to 207 MPa) into a well-designed microchannel (Y or Z type, diameter $< 100 \mu\text{m}$). Extremely high shear rates ($\dot{\gamma} \sim 10^8 \text{ s}^{-1}$) could produce uniform materials with a very small size [12]. Therefore, it has been widely used for the fabrication of nanosuspensions, such as polymer nanoparticles [13] and carbon nanotubes [14]. After

100 cycles of this procedure, Karagiannidis et al. exfoliated graphene flakes with the mean lateral size around $1 \mu\text{m}$ and mean thickness of $\sim 19 \text{ nm}$ [12]. However, the significantly increased intensity ratio of the *D* to *G* peaks ($I(D)/I(G)$) suggested smaller sheet diameter and a greater degree of defects. Therefore, to meet the enormous industrial potential application, microfluidization for quality-controllable graphene preparation requires further improvement.

Gas can provide considerable potential energy because of its compressibility. Recently, Reza et al. [15] have found a pure gas-phase method named compressible flow exfoliation (CFE). The layered materials were suspended in high-pressure gas and undergoing expansion to produce 2D nanosheets. According to fluid dynamic calculation, sufficient shear rates ($> 10^5 \text{ s}^{-1}$) formed in narrow orifices and converging–diverging channels can stimulate the exfoliation of raw layered materials mixed with the gas. The shear force produced by high-speed, gradient and compressed gas (higher than 1000 m/s) played the rule in the exfoliation, rather than the molecular interpolation stated in the previous studies on supercritical gas-assisted methods [16–18]. The huge potential energy of compressed gas allowed the processing time to be shortened to the second scale (about 2 s). Although the final yield after one preparation cycle is less than those of most liquid-phase exfoliation methods, introducing gas phase into the top-down graphene manufacturing is still worth expecting.

Herein, we developed a newly synergistic strategy (DPE method) to fabricate a time-saving, high yield (70.25%) and size-controllable graphene preparation technology, combining the microfluidization process (liquid-phase, LP, process) and supercritical CO_2 process (gas-phase, GP, process). The graphene flakes prepared by this method were mostly in form of monolayer and few-layer sheets. And the graphene dispersion still presented excellent dispersion stability after two months of standing. Besides, this method is environmentally friendly and has characterized by high yield (70.25%, 941.04 g per day theoretically), which has important guiding significance for scalable manufacturing and long-term development of graphene. Furthermore, the intercalating mechanism of the supercritical CO_2 was analyzed by molecular dynamic (MD) simulation.

Experimental section

Materials

Graphite flakes with high purity was purchased from Nanjing XFNANO Materials Tech. Co., Ltd. (China). Polyvinylpyrrolidone (PVP, P110611) was purchased from Shanghai Aladdin Biochemical Technology Co., Ltd. (China). Analytical-grade ethanol was purchased from Rionlon Bohua Pharmaceutical Chemistry Co., Ltd. The water mentioned in all experiments was deionized water.

DPE method fabricated graphene

The DPE method (Fig. 1) involves alternating microfluidization process (liquid-phase, LP, process) and supercritical CO₂ process (gas-phase, GP, process), namely LP–GP–LP process. The graphite with a size of 100 mesh and polyvinylpyrrolidone (PVP) were mixed with 0 ~ 60 vol% ethanol aqueous solution. PVP is a linear homopolymer which is soluble in water and many other polar solvents. Prior studies indicated that PVP can adsorbed on the surface of graphene to improve dispersion stability [19–22]. The average molecular weight (MW) of PVP used in this study is about 10,000 (small MW), because larger MW creates higher viscosity for the dispersion. Then higher viscosity leads to higher heat, which may cause the failure of the PVP and solvent evaporation. In our experiments, the graphite concentration C_i (10 mg/mL) and PVP concentration C_{PVP} (10 mg/ml) were selected as typical match. First, the mixture was processed 20 cycles at a typical pressure (100 MPa) by microfluidization homogenizer (LP process) with a Y-type geometry diamond

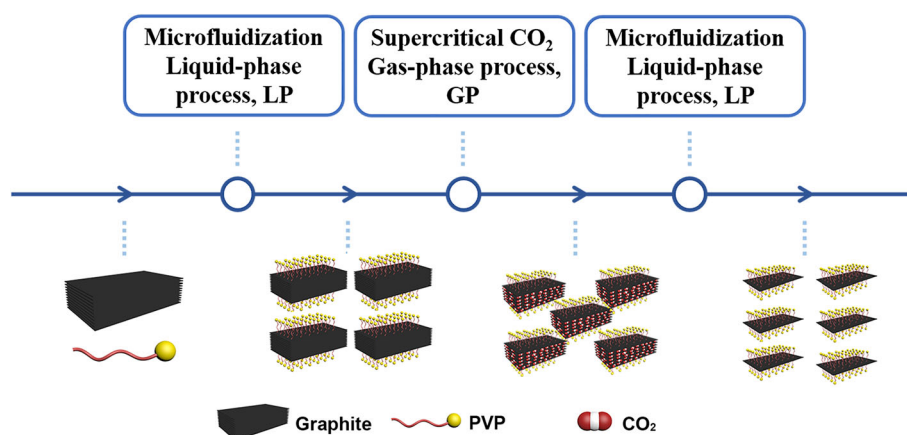
interaction chamber (F20Y-RT, Genizer), as shown in Fig. S2a. Before injecting into the chamber, the temperature of the mixture was controlled around 303 K by a cooling system. Subsequently, the mixture was transferred into a supercritical carbon dioxide (ScCO₂) reactor (Fig. S2b) and heated to 313.2 K by a heating jacket. Then liquid CO₂ was pumping into the reactor to 20 MPa under stirring. After a reaction of 3 h, the mixture was taken out and ultrasonicated in an ice bath for 30 min to discharge CO₂ gas from the solvent. Next, the microfluidization process was carried out again for 20 cycles. Eventually, the dispersion was centrifuged at a specific speed (1500 rpm, 90 min), two-thirds of which were taken for further characterization.

Characterization

A UV–Vis spectrophotometer (Shimadzu UV-1800) was used to measure the absorbance of the exfoliated graphene dispersion at 660 nm. The concentration of exfoliated graphene, C , after centrifugation was calculated using the Lambert–Beer law ($A = \alpha Cl$).

Raman spectra were measured by using a LabRAM HR Evolution (HORIBA Jobin Yvon S.A.S.) with 50 × lens and 532-nm laser. Graphene samples were prepared by freeze-dryer at 223.2 K and then were flattened on a glass substrate. A Thermo Fisher Scientific ESCALAB 250Xi X-ray photoelectron spectroscopy (XPS) system was used to perform the element analysis of the graphene film. The X-ray source gun type is an Al K Alpha. The analyzer mode of survey scans is CAE: pass energy 100 eV, and the analyzer mode of detailed scans is CAE: pass energy 20 eV.

Figure 1 A typical schematic illustration for the LP–GP–LP process of DPE method, containing alternating microfluidization (LP) and supercritical CO₂ (GP) processes. All mixtures are dispersed in an ethanol/water solution (single column).



A Bruker Dimension ICON atomic force microscope (AFM) was used to measure graphene thickness and surface morphology. The graphene sample was prepared by spin coating of the dispersion onto a silicon wafer and followed by drying at 423.2 K.

An FEI Tecnai G2 F20 S-TWIN scanning transmission electron microscope (TEM) was used to observe the graphene morphology and lattice structure. Before TEM observations, 10 μL of the dispersion was dropped onto carbon-coated grids and then dried under 353 K.

To analyze the structure of the exfoliated flakes, X-ray diffraction (XRD) experiments were conducted using a Shimadzu X-ray diffractometer (XRD-6100) with Cu K α radiation operated at 40 kV and 200 mA.

Results and discussions

Graphene prepared within different process conditions

Here, we propose a new method for graphene preparation, named the DPE method, combining microfluidization and ScCO_2 processes. A series of comparative tests were designed to evaluate efficiency to further enhance production.

One of the keys to the liquid-phase methods is the efficiency of energy utilization. Energy input in the microfluidization process (liquid-phase, LP, process) is critical to reducing the lateral and radial dimensions of graphene. Exfoliating in the microfluidization process mainly relies on the strong shear force provided by the high-speed fluid flow and pinch forces by particles colliding with each other in the interaction chamber (diameter, $d \sim 75 \mu\text{m}$, Fig. S2 a); in other words, energy could be applied to the whole fluid volume for higher efficiency [7]. In contrast, for most “top-down” methods such as high-speed shearing and ultrasound, the energy intensity depends on the position of the force sources (mixing heads and ultrasound probes), leading most of the material cannot be efficiently treated due to the energy dissipation [23, 24]. The yields by weight $Y_W = C/C_i$ are lower than 20% [6] [25], where C means the final concentration of graphene and C_i means the initial concentration of graphite. Oxidation or other chemical treatments will not be discussed here, because of the introduction of other functional groups on graphene. Herein, we compare the

efficiencies of these three methods, that are, microfluidization process, high-speed shearing and ultrasound methods. (The experimental parameters are shown in Table S1.) As shown in Fig. S1, after high-speed shearing, most of the graphite flakes were still in large size. After 24 h standing, the obvious precipitation was observed. In contrast, the dispersion prepared by the microfluidization method was stable and most graphite flakes were effectively exfoliated to small size. The concentration of the graphene C could be calculated by Beer–Lambert law: $A/l = \alpha C$, A/l states the light absorption (A) in a medium over a certain distance (l). The extinction coefficient (α) is specific to a particular 2D layered material, solvent and wavelength. (For graphene, $\alpha = 1390 \text{ mL/mg} \cdot \text{m}$ in surfactant/water solution.) After centrifugation (1500 rpm for 90 min), the C is 1.221, 0.16 and 0.091 mg/mL, for 30 min of microfluidization method, ultrasound and high-speed shearing method, respectively (Fig. 2a). The higher concentration indicates microfluidization is an ideal method for graphene preparation as compared with typical “top-down” methods [12, 15, 26, 27]. The effect of initial graphite concentration (C_i) in the LP process was subsequently explored. Usually increased initial graphite concentration (C_i) could increase final output for traditional liquid-phase methods [8, 28]. Figure 2b indicates that C increases with the increase in C_i . However, C decreased when the C_i was up to 10 mg/ml. With the increase in the graphite concentration, the contact between graphite and liquid medium will be relatively reduced. Therefore, production cannot be enhanced by simply increasing initial graphite concentration (C_i), which was set to 10 mg/ml for all experiments in this study.

Excessive homogenization will cause severe fragmentation (nanometer size in radial direction) of graphene [8, 12, 22, 29], reducing the actual performance because of the strong size dependence in applications [5, 30]. To reduce excessive fragmentation, introducing mild gas phase like supercritical CO_2 (ScCO_2) into the “top-down” processes is gaining considerable attraction [15, 17, 21, 31]. According to Pu et al. [32] and Rangappa et al. [17], ScCO_2 , owing to high diffusivity, expansibility and solvating power, could weak van der Waals force by intercalating into graphite spacing, named the intercalation mechanism. Relatively, Xu et al. [21] proposed micelles can be turned to reverse micelles in the emulsion microenvironment consisting of ScCO_2 and

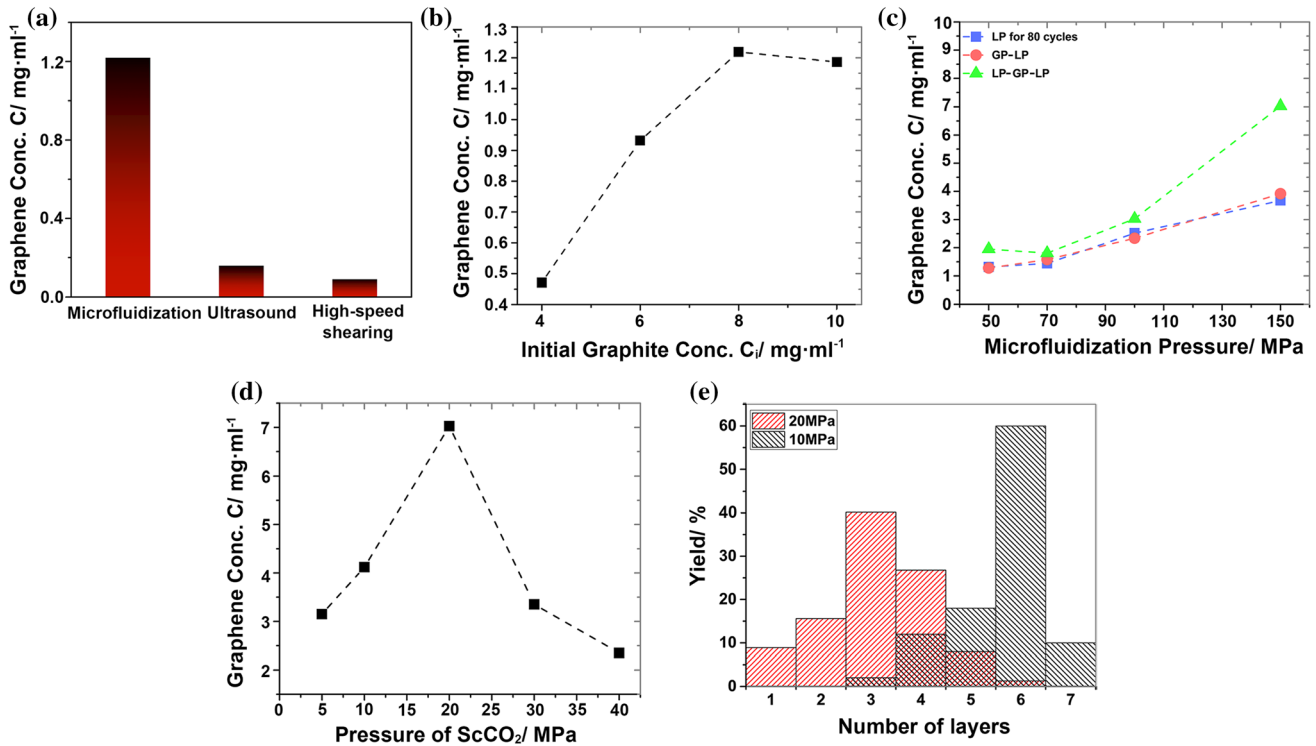


Figure 2 a Efficiency of microfluidization and other two typical “top-down” methods for exfoliating graphene. b Plots showing the effects of initial graphite concentration (C_i) in the microfluidization process. c Graphene concentration in LP, GP-LP and LP-GP-LP process with the microfluidization pressure from 50 to 150 MPa.

d Plots showing the effects of pressure of CO₂ on the final concentration of graphene in the LP-GP-LP process. e Histogram of layers for graphene treated with ScCO₂ in the GP process. The pressures of ScCO₂ are 10 MPa and 20 MPa, respectively (2 columns).

PVP. The force due to curvature change will tear the graphene off the graphite, named the Micellar transformation mechanism. Based on these two mechanisms, the ScCO₂ process (GP) is an ideal gentle method for graphene preparation without excessive fragmentation. Herein, we try to graft the ScCO₂ process (GP) into the microfluidization process (LP). The typical DPE method is designed as LP-GP-LP; that is, the ScCO₂ process is placed between two independent microfluidization processes. Meanwhile, single microfluidization process and “one microfluidization process + one ScCO₂ process,” named LP and GP-LP, were designed as a comparison. Figure 2c shows the difference in production efficiency under different combinations. With the increase in LP pressure from 50 MPa to 100 MPa, the concentration of graphene increases. Obviously, the greater the strength of the LP process, the greater the shear rate, which will inevitably lead to a higher yield. However, when the pressure in LP increases up to 150 MPa, the LP-GP-LP process showed a huge improvement, in which the pressure of ScCO₂

(GP) was controlled in 20 MPa. The C reached 7.025 mg/ml, whose yield up to 70.25%. The processing capacity of industrial-grade equipment is 240 L per hour. The flakes production (P_r) is equal to $\left(\frac{M_{\text{Graphite}}}{t}\right) \times 70.25\%$ (g/h). For a typical batch ($M_{\text{Graphite}} = 2400\text{g}$ and $t = 43\text{h}$, including 40 h for the LP process and 3 h for the GP process), $P_r = \sim 39.21\text{g/h}$, that is, 941.04 g per day.

The change in production efficiency must be related to the introduction of the GP process. Then, we studied the correlation between exfoliation efficiency and parameters in the GP process. Figure 2d shows that with the increases in the pressure of ScCO₂, C first increases and then decreases. It indicates that the intercalation mechanism and the Micellar transformation mechanism existed simultaneously during the exfoliation process, leading to the existence of an optimal pressure of ScCO₂ for yield [33]. Also, the content of ethanol in the system can affect C (shown in Fig. S3), suggesting that in the ScCO₂ process, the exfoliation efficiency is related to the solution

composition [17, 21, 33, 34]. It is worth noting that the compositions of the solvents (water:ethanol) were not constant. Under the experimental conditions, the microfluidization process (LP) generates significant frictional heat, despite the presence of a cooling device. For the ScCO₂ process (GP), the addition and release of carbon dioxide are accompanied by changes in system pressure and temperature. All these led to the changes in the solvent composition of the system. However, we believe that in the entire process, the surface energy of the mixed system matches the surface energy required for exfoliating graphene [35].

Morphology and structural of exfoliated graphene

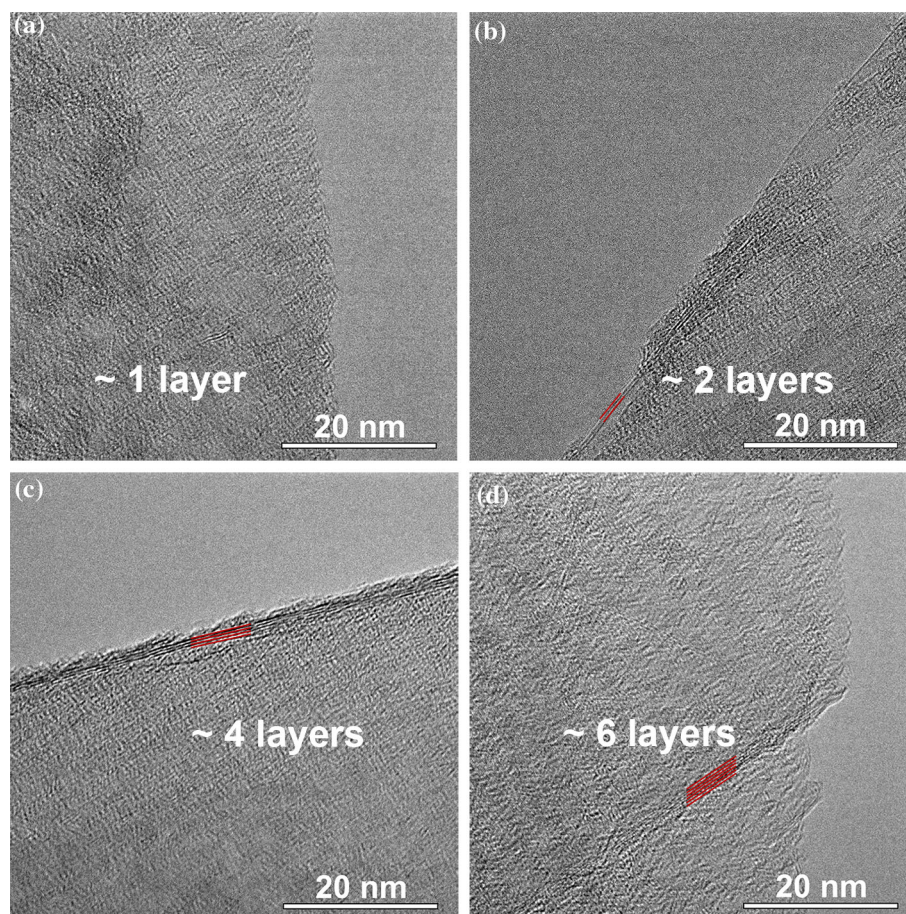
As current commercial applications of graphene are highly sensitive to product quality, improving the quality control of graphene products is critical [5]. Large-size graphene has advantages in certain applications, such as thermal conductivity [36]. Herein, transparent wrinkled graphene nanosheets with micron size were prepared by the DPE method, as shown in Fig. 4a. We also calculated the lateral size of graphene prepared by the typical LP–GP–LP process. As shown in Fig. S4, most of the lateral size is distributed in 0.6–1.2 microns. There are ~ 41% graphene sheets larger than 1 micron. This indicates that while ensuring efficient production, the mild GP process ensures the lateral size of graphene nanosheets. The number of layers is another important quality evaluation index, usually calculated by counting the number of dark lines on the curled graphene edges. Representatively higher-magnification TEM images of obtained graphene are shown in Fig. 3. Edges with different dark lines (e.g., 1 in Figs. 3a and 2 in Fig. 3b) suggest single- and few-layer graphene [37].

High-resolution transmission electron microscope (HRTEM) images suggest the hexagonal lattice pattern (Fig. 4b). After further Fourier and inverse Fourier transforms, a clear and complete hexagonal network pattern was obtained, as shown in Fig. 4c, suggesting a well-preserved in-plane lattice structure of graphene. The brightness contrast in the TEM images corresponds to different thicknesses [35]. By analyzing the electron diffraction pattern, a more definitive identification of graphene can be made [38]. Figure 4e, f shows SAED of the white and black

dots in Fig. 4d, respectively. The pattern in Fig. 4e shows a typical sixfold symmetry, labeled by Miller–Bravais indices. The inner peaks ((0–110) and (–1010)) are more intense than the outer ones, that is, the $I_{[1100]}/I_{[2110]} > 1$, confirming the sheet marked by white dot is a monolayer. However, the pattern marked by black dot shows two staggered concentric hexagonal, confirming graphene sheets with rotational stacking, which is different from the standard AB Bernal packing of bulk graphite [39]. Therefore, it can be determined that graphene sheets in Fig. 4d were completely peeled off and then stacked again. Atomic force microscopy (AFM) height profile shows the nanosheet is around 1.27 nm thick (Fig. 4g, h and i). It has been reported that the thickness of a single-layer graphene on a silicon wafer was about 0.75 nm due to the roughness and cleanliness of the silicon wafer [40].

Raman spectroscopy, X-ray photoelectron spectroscopy (XPS) and XRD were conducted to evaluate the structural of graphene. Figure 5a shows the Raman spectra of graphite and few-layer graphene with 532-nm laser. The graphene sample is prepared by the LP–GP–LP process. A sharp and symmetrical single Lorentz peak at 2675.31 cm⁻¹ corresponding to the typical 2D peak of a graphene nanosheet confirms the monolayer structure of graphene [41]. The peak at around 1575 cm⁻¹ refers to the G band which is assigned to the E_{2g} mode of sp² hybridized carbon bonds, while the peak at around 1340 cm⁻¹ refers to the D band which is associated with the breathing mode of k-point phonons of A_{1g} symmetry. Whereas D band is usually activated by defect degrees such as edges, functional groups, the $I(D)/I(G)$ and Peak D value allow us to judge the structural integrity of graphene [12, 42]. Figure 5b shows representative spectra of the starting graphite and graphene exfoliated by different homogeneous pressure. The $I(D)/I(G)$ increases from 0.08 to 1.26, which means smaller size [9, 12]. What is more, $I(D)/I(D')$ was 1, 2.45, 3.27 and 3.6 for 20, 70, 140 and 200 MPa, respectively. Considering that the $I(D)/I(D')$ of the original graphite was about 1, it can be determined that there were no additional vacancy defects and SP³ defects during the manufacturing process [8]. Therefore, for a typical DPE method, the homogeneous pressure was ≤ 150 MPa, which made $I(D)/I(G) < 0.5$. The higher value of D peak may be caused by the sp³ C element in the residual PVP on the surface of

Figure 3 TEM images of graphene edges with different layers. **a** 1 layer, **b** 2 layers, **c** 4 layers and **(d)** graphene with 6- and single-layer stacks (single column).



graphene [20], though this has no effect on the overall trend.

It is important to evaluate chemical changes in the sample, such as excessive oxidation or functionalization, which may lead to inferior qualities [5, 43]. The element proposition of as-prepared graphene was revealed by XPS (Fig. 5c), C_{1s} (96.33%), N_{1s} (1.26%) and O_{1s} (2.41%). The ultra-high C_{1s}/O_{1s} (39.97) is much higher than graphene oxide (GO) or reduced graphene oxide (rGO) (lower than ~ 15) [44, 45]. The deconvolution of the high-resolution C_{1s} spectrum to the C–C band, C–N band and C=O band. The weak signals of C–N and C=O refer to the residual of surfactant (Fig. 5d). Therefore, no excessive oxidation or functionalization has occurred to change the chemical composition of the graphene samples during the DPE process. XRD patterns of graphite powder and water-washed graphene nanosheets are shown in Fig. 5e. A sharp intense diffraction peak at $2\theta = 26.52^\circ$ is associated with (002) diffraction characteristic of the graphite (d -spacing = 0.34 nm), and the weakened 002 peaks indicate

that the exfoliated graphene remained the original pristine structure. However, the new broad diffraction peak appears at 21.78° correspond to an expanded interlayer spacing of 0.41 nm, which may be resulted by the intercalation CO₂ molecule.

We also explored the dispersion stability of the graphene dispersion. With the help of PVP, the graphene dispersion made by a typical DPE method had good stability at room temperature and normal pressure. The black aqueous solution had no obvious color difference after about two months, as shown in Fig. 6. The samples in supernatant from day 0 and day 57 were measured by AFM. The results indicate that bilayer graphene sheets were significantly increased after 57 days standstill, which may be caused by the settlement of thicker sheets and agglomeration of monolayers.

Preparation mechanism of DPE method

In this study, we achieved high efficiency (yield up to ~ 70.25%), while ensuring a large graphene sheet

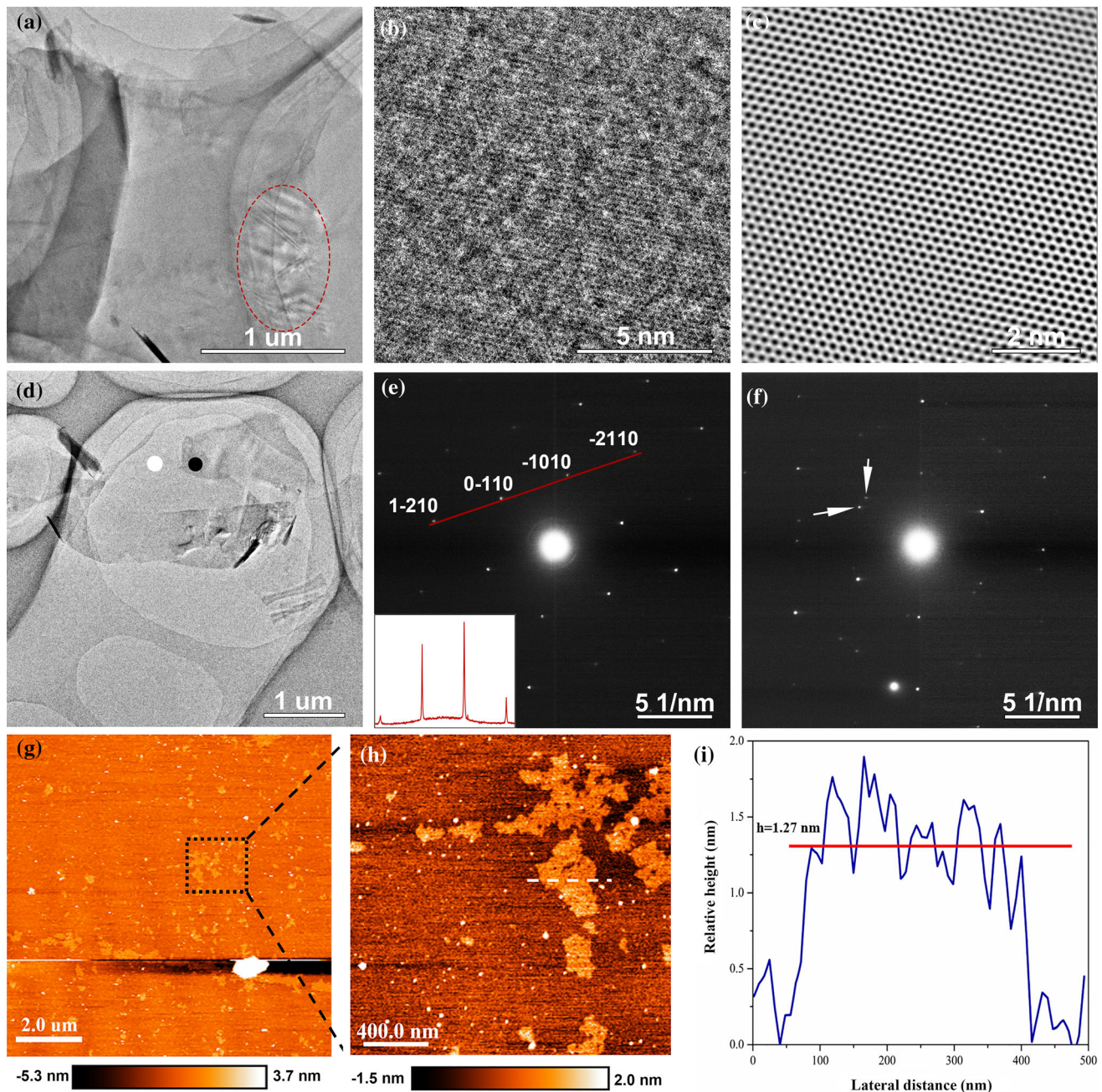


Figure 4 **a** TEM images of pieces of graphene with the size around 1 μm . **b** HRTEM image of the red circle in **(a)**. **c** A filtered image of **(b)**. **d** TEM image of two pieces of single-layer graphene stacked on top of each other. **e**, **f** SAED patterns of the white dot

and the black dot in **(d)**, respectively. **g**, **h** Typical AFM image of exfoliated graphene nanosheets. **(i)** Height test of the dotted part in **(h)** (2 columns).

(micron-level diameter) by introducing the ScCO_2 process (GP). A synergy between microfluidization process (LP) and ScCO_2 process (GP) must play essential roles in the DPE method, leading that exfoliating efficiency is sensitive to process sequence. The comparisons of production efficiency with other “top-down” methods are shown in Fig. S5. To explain

the synergy between the relatively strong microfluidization process (LP) and the mild ScCO_2 process (GP), Fig. 7a proposes the mechanism of the DPE method. In the first LP process, bulk graphites were homogenized (20–30 cycles) to small sheets (as shown in Fig. S1c) by strong shear force. The PVP with hydrophobic functional groups adsorbed on the

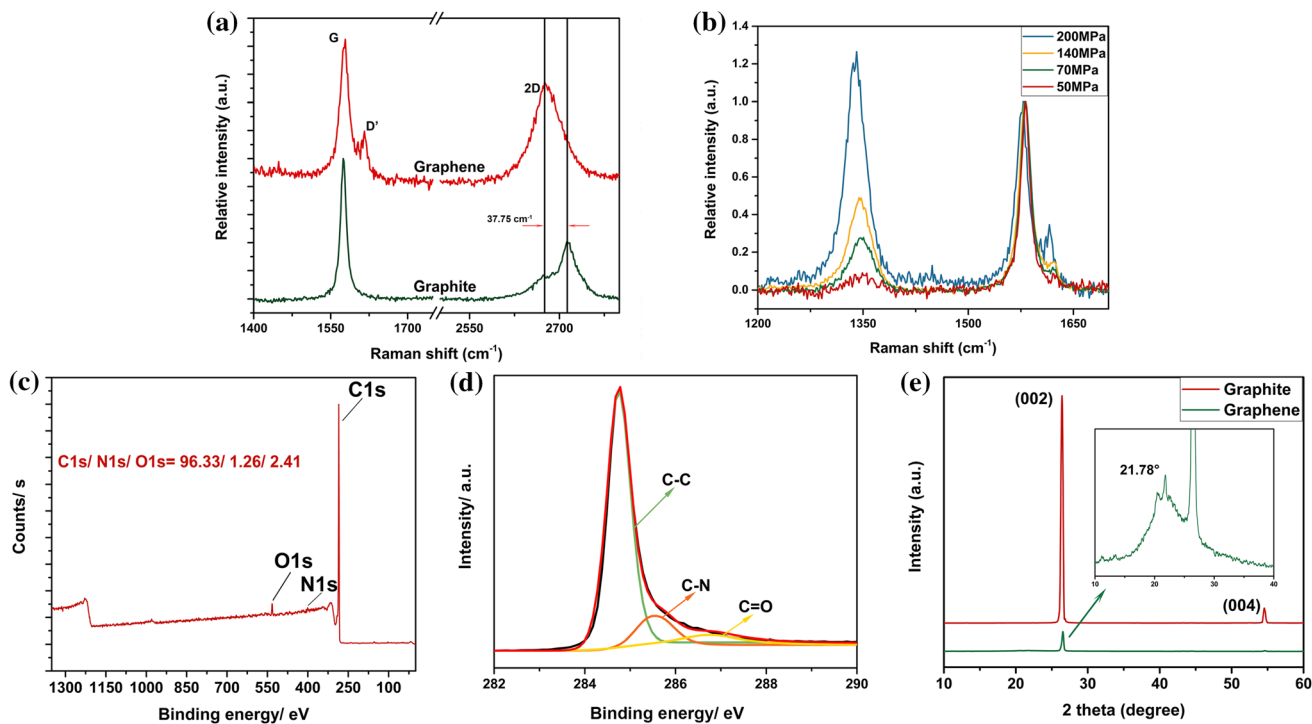


Figure 5 a, b Raman spectra of graphite powder and graphene nanosheets with different thickness (a) and defect level (b). c–e XPS survey (d) and high-resolution C_{1s} spectra (e) of graphene

surface of the fragments meanwhile to prevent reaggregation. Subsequently, the mixture was placed in a ScCO₂ reactor, in which the pumped liquid carbon dioxide will gradually reach the supercritical state (20 MPa, 40 ~ 45 °C). Supercritical carbon dioxide molecules would dissolve into the mixture [34, 46, 47] and insert into the graphite layers. At the same time, the reverse micelle transformation proceeds cause the surface graphite layer to be stripped due to the curvature change. After CO₂ molecules releasing, the last LP process is applied to expand graphite and for further exfoliation. Overall, the synergy between the microfluidization process (LP) and the ScCO₂ process (GP) in the DPE method is as follows: (a) Appropriate homogeneity parameters enable shear graphite to smaller fragments and (b) the ScCO₂ process subsequently increases the production of graphene mildly and expands the graphite layer spacing, which could further expand the exfoliating efficiency of the last microfluidization process (LP).

For liquid-phase exfoliation, the energy output was closely related to fluid motion, so hydrodynamics in the microchannel was elucidated. The Reynolds

prepared by the LP–GP–LP method. (f) XRD patterns of graphite powder and water-washed graphene nanosheets (2 columns).

number (*Re*) in the microchannel can be used to judge the type of the flow, which is related to the exfoliating efficiency [9], and it is given by [48]

$$Re = \frac{\rho UD}{\mu}$$

where ρ [kg/m³] is the liquid density (the mixture contained 10 mg/mL of graphite, 10 mg/mL of PVP, 40–50 vol % of ethanol and water, corresponding to a total density of 990 kg/m³). The mean velocity *U* (m/s) of the fluid inside the microchannel was 377–400 m/s, which be controlled by changing microfluidization pressure. And the dynamic viscosity μ [Pa·s] was 1×10^{-3} Pa·s, which was measured by a rotational rheometer. Therefore, with the fixed diameter of the microchannel *D* (~ 75 μ m), we can roughly estimate *Re* up to 2.8×10^8 , which suggests a total turbulence. Collision between the graphite and the hard geometric microchannel can also produce tiny fragments, but it is limited for graphene exfoliation because the direction of the force cannot be controlled to parallel to the graphite surface [9, 49]. In the microchannel, the radial velocity distribution is generally a parabolic profile. Moreover, the boundary layer next to the solid wall has a huge velocity

Figure 6 **a, b** Histograms of the thickness of graphene sheets of the supernatant in day 0 and day 57 counted by AFM. The counted number, N , is 100. **c** Digital photographs of graphene aqueous solution of days 0, 7, 21 and 57 (single column).

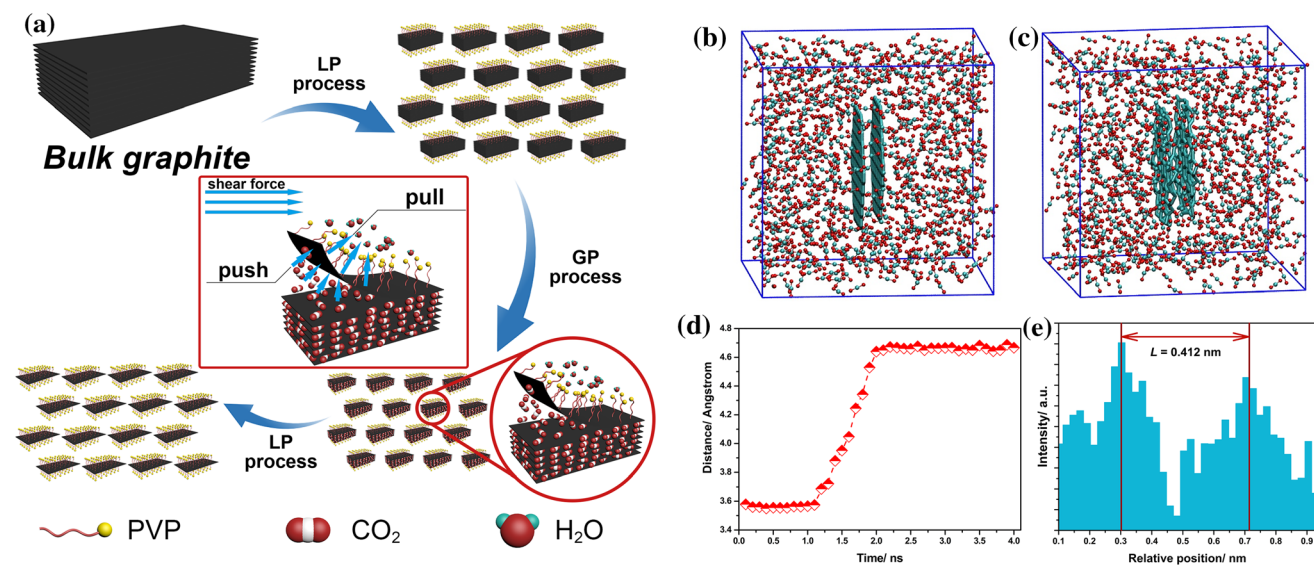
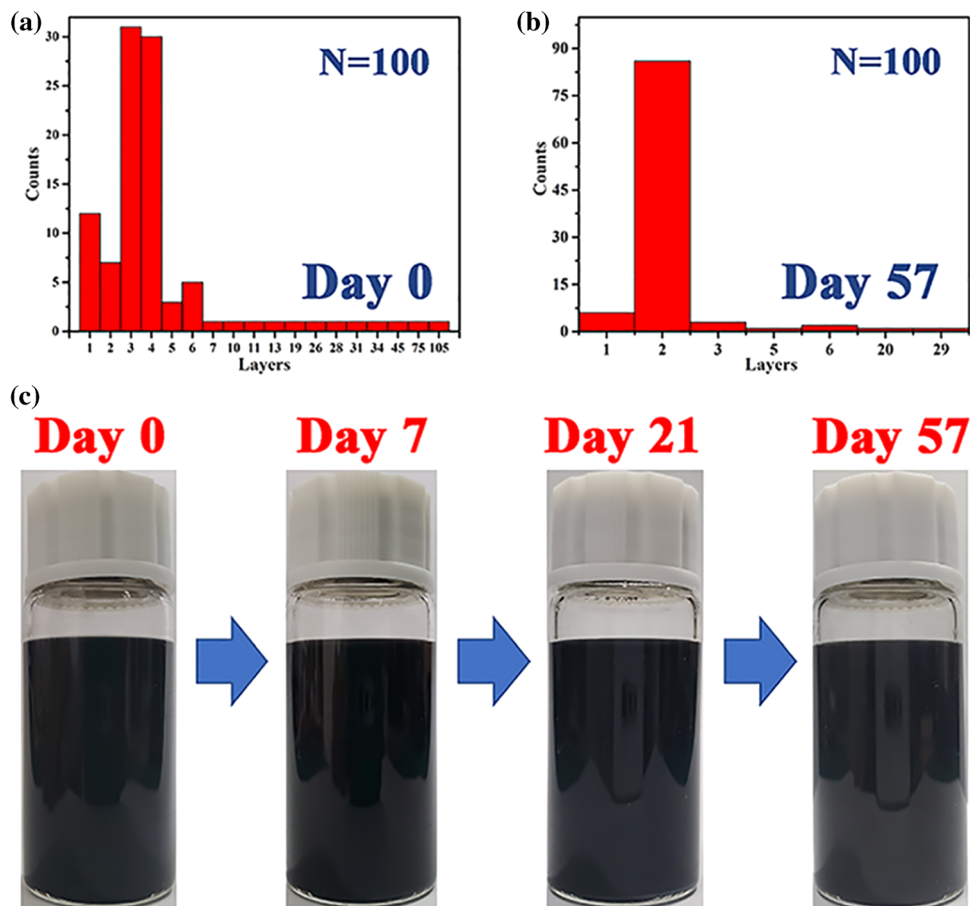


Figure 7 **a** Possible mechanism of DPE method. The inset in the middle of the figure lists the possible forces during preparation. In particular, these forces did not work at the same time, but separately in the LP process and GP process respectively. **b, c** Representative configurations of the graphene sheets and CO₂

molecules before and after the equilibrium MD simulation, respectively. **d** Variation curve of layer spacing during the equilibrium MD simulation. **e** Intensity profile perpendicular to the red line in Fig. 3b (2 columns).

gradient. Shear force parallel to the graphite surface played the role for exfoliation [9]. When the turbulence was fully developed, the huge exchange energy of randomly vortices cannot be ignored at the same time. The shear rate provided by the flow can reach to 10^8 s^{-1} [12], which was much higher than the required shear rate ($\sim 10^4 \text{ s}^{-1}$) to initiate graphite exfoliation [8]. Under such strong interactions, the bulk graphite was easily sheared to graphene, and the adsorbed PVP can further prevent agglomeration.

In the GP process, not the force parallel to the graphite sheet layer, but the force perpendicular to the graphite sheet contributes to exfoliation. Micelles can turn to reverse micelles in the emulsion microenvironment when carbon dioxide reaches a certain pressure in a water/PVP solution system [21, 47, 50, 51]. Due to the relatively strong interaction between PVP and graphite, the curvature change (GP process in Fig. 7a) of the micelles provided driving forces for exfoliating, which includes the push force by carbon dioxide molecules and the draw force by water molecules. Contrary to the liquid-phase process, the reverse micelle switching was slow [21, 51], leading a weak driving force and hardly causing damage to the graphite sheet. This explains that when the pressure in the first LP process reaches a certain value, the final graphene yield increased sharply, because the Micellar transformation was only effective when the sheets diameter was small enough. When ScCO_2 was introduced to the emulsion system, the phase behavior of the emulsion microenvironment can be described as follows: (a) The increased pressure facilitates the carbon dioxide gradually dissolving into the continuous phase of PVP / water, which causes the formation of CO_2 -in-water emulsions under the action of hydrophilic amide groups of PVP [21]; (b) when the CO_2 reaches the supercritical state (20 MPa and $40 \sim 45 \text{ }^\circ\text{C}$ in this study), the gas molecular penetrates the interlayer of graphite with a high diffusivity [31], increasing the distance and reducing the interaction between adjacent layers; (c) with the increasing number of carbon dioxide molecules, the hydrophobic core gradually increases; and (d) eventually, a reverse micelle with water as the core is formed under the repulsive forces between hydrophilic amide groups and CO_2 [33, 34]. Through the curvature transition during the Micellar transformation, the single or few layers of graphene are exfoliated because of the strong hydrophobic interaction between surfactant and graphite.

Figure 2e indicates the average thickness of graphene decreases with the increase in the pressure of ScCO_2 , and an increasing ScCO_2 density can enhance the dispersion stability of samples by providing the higher free energy barrier and weakening van der Waals force between them [16]. However, with CO_2 molecules increasing, the gas molecules would be inserted between the PVP segments, leading the curvature of the micelle decreasing [33] and then reducing the driving force for “pulling” graphene. Therefore, as shown in Fig. 2d, when the carbon dioxide pressure exceeds a certain value, the graphene output will decrease.

Molecular dynamic (MD) simulations are applied to perform the intercalation mechanism. All the all-atom MD simulations were based on OPLS-AA force field [52] and carried out using the Gromacs-4.6.7 software package [53]. The carbon atoms of the graphene sheet (150 carbon atoms) were treated as uncharged particles interacting through the Lennard–Jones (L–J) potential with $\sigma = 0.391 \text{ nm}$ and $\varepsilon = 0.14115 \text{ kJ/mol}$ [54]. The CO_2 molecules were put in the simulation box with the CO_2 experimental critical density (0.950 g/cm^3 , equivalent to 40 MPa) [55]. The system is a relaxed liquid configuration at 313 K. The time step was 2 fs, and the total run time was 4 ns for the equilibrium MD simulation in the canonical ensemble (NVT). As it is before system relaxation MD, energy minimization was carried out with a composite protocol of steepest descent using termination gradients of 100 kJ/mol nm . The Nose–Hoover thermostat [56] was used to maintain the equilibrium temperature at 313 K and periodic boundary conditions were imposed on all three dimensions. The particle mesh Ewald method [57, 58] was used to compute long-range electrostatics within a relative tolerance of 1×10^{-6} . A cutoff distance of 1 nm was applied to real space Ewald interactions. The same value was used for van der Waals interactions. The LINCS algorithm [59] was applied to constrain bond lengths of hydrogen atoms. A leap frog algorithm [60] was used with a time step of 2 fs. Figure 7b and c shows the initial configuration on the left and the final configuration on the right. The graphene becomes wrinkled, and the interlayer distance is slightly enlarged after relaxation. More importantly, parts of the carbon dioxide molecules are inserted between the sheets. More details of the change in the interlayer spacing of graphite are shown in Fig. 7d, from 3.6 to 4.6 Å, which shows that

carbon dioxide does expand the interlayer spacing of graphite layers. Figure 7e shows the intensity profile perpendicular to the red line in Fig. 3b, suggested an interlayer distance of 0.412 nm, which is larger than that of typical graphite, 0.335 nm, and consistent with the simulation results.

Conclusion

In summary, we proposed a new graphene exfoliating method based on a dual-phase system, which were the microfluidization process (liquid-phase, LP) and supercritical carbon dioxide process (gas-phase, GP), namely dual-phase exfoliating (DPE) method. First, graphite was quickly broken and exfoliated under a homogeneous microjet. Then supercritical carbon dioxide diffused into the graphite layers and formed reverse micelles on the graphite surface by changing the polarity of the system. In the end, the mixture was further sheared into thinner pieces by the final LP process. The concentration of the graphene dispersion reaches 7.025 mg/ml, which means the yield can achieve a high level with 70.25%. It is worth noting that the homogenization pressure and the carbon dioxide pressure can adjust the yield, degree of defect and thickness of the graphene. In the scale-up production, it is expected to achieve more accurate quality control through fine fluid mechanic calculation and process design. Through molecular dynamic (MD) simulation, the intercalation phenomenon of carbon dioxide under a supercritical state was studied. This work is expected to provide new ideas for large-scale, quality-controllable and environmentally friendly grapheme top-down manufacturing, which will further promote the application of graphene in nanofilms, conductive inks and coating additions.

Acknowledgements

This work was supported by the National Natural Science Foundation of China [Grant 51875549, 51935012, 51935006]; the Youth Innovation Promotion Association of Chinese Academy of Sciences [2018457]; and the Key Research Program of Frontier Science, Chinese Academy of Sciences [Grant QYZD]-SSW-SLH056].

Compliance with ethical standards

Conflict of interest The authors declare that they have no conflict of interest.

Supplementary Information: The online version of this article (<https://doi.org/10.1007/s10853-021-05903-4>) contains supplementary material, which is available to authorized users.

References

- [1] Lee C, Wei X, Kysar JW, Hone J (2008) Measurement of the elastic properties and intrinsic strength of monolayer graphene. *Science* 321:385–388
- [2] Balandin AA, Ghosh S, Bao W, Calizo I, Teweldebrhan D, Miao F, Lau CN (2008) Superior thermal conductivity of single-layer graphene. *Nano Lett* 8:902–907
- [3] Xu Y, Lin Z, Zhong X, Huang X, Weiss NO, Huang Y, Duan X (2014) Holey graphene frameworks for highly efficient capacitive energy storage. *Nat Commun* 5:1–8
- [4] Zhang Y, Tang T-T, Girit C, Hao Z, Martin MC, Zettl A, Crommie MF, Shen YR, Wang F (2009) Direct observation of a widely tunable bandgap in bilayer graphene. *Nature* 459:820–823
- [5] Lin L, Peng H, Liu Z (2019) Synthesis challenges for graphene industry. *Nat Mater* 18:520–524
- [6] Tao H, Zhang Y, Gao Y, Sun Z, Yan C, Texter J (2017) Scalable exfoliation and dispersion of two-dimensional materials—an update. *Phys Chem Chem Phys* 19:921–960
- [7] Witomska S, Leydecker T, Ciesielski A, Samori P (2019) Production and patterning of liquid phase-exfoliated 2D sheets for applications in optoelectronics. *Adv Function Mater* 29:1901126
- [8] Paton KR, Varrla E, Backes C, Smith RJ, Khan U, O'Neill A, Boland C, Lotya M, Istrate OM, King P (2014) Scalable production of large quantities of defect-free few-layer graphene by shear exfoliation in liquids. *Nat Mater* 13:624
- [9] Arao Y, Mizuno Y, Araki K, Kubouchi M (2016) Mass production of high-aspect-ratio few-layer-graphene by high-speed laminar flow. *Carbon* 102:330–338
- [10] Varrla E, Paton KR, Backes C, Harvey A, Smith RJ, McCauley J, Coleman JN (2014) Turbulence-assisted shear exfoliation of graphene using household detergent and a kitchen blender. *Nanoscale* 6:11810–11819
- [11] Wang J, Manga KK, Bao Q, Loh KP (2011) High-yield synthesis of few-layer graphene flakes through electrochemical expansion of graphite in propylene carbonate electrolyte. *J Am Chem Soc* 133:8888–8891

- [12] Karagiannidis PG, Hodge SA, Lombardi L, Tomarchio F, Decorde N, Milana S, Goykhman I, Su Y, Mesite SV, Johnstone DN (2017) Microfluidization of graphite and formulation of graphene-based conductive inks. *ACS Nano* 11:2742–2755
- [13] Panagiotou T, Mesite S, Bernard J, Chomistek K, Fisher R (2008) Production of polymer nanosuspensions using microfluidizer processor based technologies. In: Proceedings of the nanotechnology conference and trade show, pp 688–691
- [14] Panagiotou T, Bernard JM, Mesite SV (2008) Deagglomeration and dispersion of carbon nanotubes using microfluidizer high shear fluid processors. In: Nano science and technology institute (NSTI) conference and expo proceedings, pp 39–42
- [15] Rizvi R, Nguyen EP, Kowal MD, Mak WH, Rasel S, Islam MA, Abdelaal A, Joshi AS, Zekriardehani S, Coleman MR, Kaner RB (2018) High-throughput continuous production of shear-exfoliated 2d layered materials using compressible flows. *Adv Mater* 30:11
- [16] Wu B, Yang X (2011) A molecular simulation of interactions between graphene nanosheets and supercritical CO₂. *J Colloid Interface Sci* 361:1–8
- [17] Rangappa D, Sone K, Wang M, Gautam UK, Golberg D, Itoh H, Ichihara M, Honma I (2010) Rapid and direct conversion of graphite crystals into high-yielding, good-quality graphene by supercritical fluid exfoliation. *Chem–A Eur J* 16:6488–6494
- [18] Li L, Zheng X, Wang J, Sun Q, Xu Q (2012) Solvent-exfoliated and functionalized graphene with assistance of supercritical carbon dioxide. *ACS Sustain Chem Eng* 1:144–151
- [19] Zhu H, Zhang C, Tang Y, Wang J, Ren B (2007) Preparation and thermal conductivity of suspensions of graphite nanoparticles. *Carbon* 45:226–228
- [20] Wajid AS, Das S, Irin F, Ahmed HST, Shelburne JL, Parviz D, Fullerton RJ, Jankowski AF, Hedden RC, Green MJ (2012) Polymer-stabilized graphene dispersions at high concentrations in organic solvents for composite production. *Carbon* 50:526–534
- [21] Xu S, Xu Q, Wang N, Chen Z, Tian Q, Yang H, Wang K (2015) Reverse-micelle-induced exfoliation of graphite into graphene nanosheets with assistance of supercritical CO₂. *Chem Mater* 27:3262–3272
- [22] Guardia L, Fernández-Merino M, Paredes J, Solis-Fernandez P, Villar-Rodil S, Martínez-Alonso A, Tascón J (2011) High-throughput production of pristine graphene in an aqueous dispersion assisted by non-ionic surfactants. *Carbon* 49:1653–1662
- [23] Santos HM, Lodeiro C, Capelo-Martinez J-L (2009) *Ultrasound in chemistry: analytical applications*. Wiley, NJ
- [24] Atiemo-Obeng VA, Calabrese RV (2004) Rotor-stator mixing devices. In: *Handbook of industrial mixing: science and practice*. Wiley, pp 479–505
- [25] Bonaccorso F, Lombardo A, Hasan T, Sun Z, Colombo L, Ferrari AC (2012) Production and processing of graphene and 2d crystals. *Mater Today* 15:564–589
- [26] Paton KR, Anderson J, Pollard AJ, Sainsbury T (2017) Production of few-layer graphene by microfluidization. *Mater Res Express* 4:025604
- [27] Xu Y, Chen S, Dou Z, Ma Y, Mi Y, Du W, Liu Y, Zhang J, Chang J, Liang C, Zhou J, Guo H, Gao P, Liu X, Che Y, Zhang Y (2019) Robust production of 2D quantum sheets from bulk layered materials. *Mater Horizons*. <https://doi.org/10.1039/C9MH00272C>
- [28] Lotya M, Hernandez Y, King PJ, Smith RJ, Nicolosi V, Karlsson LS, Blighe FM, De S, Wang Z, McGovern IT, Duesberg GS, Coleman JN (2009) Liquid phase production of graphene by exfoliation of graphite in surfactant/water solutions. *J Am Chem Soc* 131:3611–3620
- [29] Zhang S-L, Zhang Z, Yang W-C (2016) High-yield exfoliation of graphene using ternary-solvent strategy for detecting volatile organic compounds. *Appl Surf Sci* 360:323–328
- [30] Peng L, Xu Z, Liu Z, Guo Y, Li P, Gao C (2017) Ultrahigh thermal conductive yet superflexible graphene films. *Adv Mater* 29:1700589
- [31] Song NN, Jia JF, Wang WC, Gao YH, Zhao YP, Chen Y (2016) Green production of pristine graphene using fluid dynamic force in supercritical CO₂. *Chem Eng J* 298:198–205
- [32] Pu N-W, Wang C-A, Sung Y, Liu Y-M, Ger M-D (2009) Production of few-layer graphene by supercritical CO₂ exfoliation of graphite. *Mater Lett* 63:1987–1989
- [33] Zhang J, Han B, Zhang C, Li W, Feng X (2008) Nanoemulsions induced by compressed gases. *Angewandte Chemie Int Ed* 47:3012–3015
- [34] Zhang J, Han B, Zhao Y, Li J, Yang G (2011) Switching micellization of Pluronics in water by CO₂. *Chem–A Eur J* 17:4266–4272
- [35] Hernandez Y, Nicolosi V, Lotya M, Blighe FM, Sun Z, De S, McGovern I, Holland B, Byrne M, Gun'Ko YK (2008) High-yield production of graphene by liquid-phase exfoliation of graphite. *Nat Nanotechnol* 3:563
- [36] Zhu Y, Ji H, Cheng H-M, Ruoff RS (2017) Mass production and industrial applications of graphene materials. *Natl Sci Rev* 5:90–101
- [37] Ni ZH, Wang HM, Kasim J, Fan HM, Yu T, Wu YH, Feng YP, Shen ZX (2007) Graphene thickness determination using reflection and contrast spectroscopy. *Nano Lett* 7:2758–2763

- [38] Meyer JC, Geim A, Katsnelson M, Novoselov K, Obergfell D, Roth S, Girit C, Zettl A (2007) On the roughness of single- and bi-layer graphene membranes. *Solid State Commun* 143:101–109
- [39] Warner JH, Rummeli MH, Gemming T, Büchner B, Briggs GAD (2009) Direct imaging of rotational stacking faults in few layer graphene. *Nano Lett* 9:102–106
- [40] Parvez K, Wu Z-S, Li R, Liu X, Graf R, Feng X, Mullen K (2014) Exfoliation of graphite into graphene in aqueous solutions of inorganic salts. *J Am Chem Soc* 136:6083–6091
- [41] Park JS, Reina A, Saito R, Kong J, Dresselhaus G, Dresselhaus MS (2009) G' band Raman spectra of single, double and triple layer graphene. *Carbon* 47:1303–1310
- [42] Ferrari AC, Basko DM (2013) Raman spectroscopy as a versatile tool for studying the properties of graphene. *Nature Nanotechnol* 8:235
- [43] Punckt C, Muckel F, Wolff S, Aksay IA, Chavarin CA, Bacher G, Mertin W (2013) The effect of degree of reduction on the electrical properties of functionalized graphene sheets. *Appl Phys Lett* 102:023114
- [44] Drewniak S, Muzyka R, Stolarczyk A, Pustelny T, Kotyczka-Morańska M, Setkiewicz M (2016) Studies of reduced graphene oxide and graphite oxide in the aspect of their possible application in gas sensors. *Sensors* 16:103
- [45] Yang D, Velamakanni A, Bozoklu G, Park S, Stoller M, Piner RD, Stankovich S, Jung I, Field DA, Ventrone CA Jr (2009) Chemical analysis of graphene oxide films after heat and chemical treatments by X-ray photoelectron and Micro-Raman spectroscopy. *Carbon* 47:145–152
- [46] Johnston K, Harrison K, Clarke M, Howdle S, Heitz M, Bright F, Carlier C, Randolph T (1996) Water-in-carbon dioxide microemulsions: an environment for hydrophiles including proteins. *Science* 271:624–626
- [47] Zhuo S, Huang Y, Peng C, Liu H, Hu Y, Jiang J (2010) CO₂-induced microstructure transition of surfactant in aqueous solution: insight from molecular dynamics simulation. *J Phys Chem B* 114:6344–6349
- [48] Munson BR, Young DF, Okiishi TH (2006) *Fundamentals of fluid mechanics*. Wiley, USA
- [49] Yi M, Shen Z (2015) A review on mechanical exfoliation for the scalable production of graphene. *J Mater Chem A* 3:11700–11715
- [50] Zhang J, Han B (2012) Supercritical or compressed CO₂ as a stimulus for tuning surfactant aggregations. *Acc Chem Res* 46:425–433
- [51] Qi Y, Xu Q, Wang Y, Yan B, Ren Y, Chen Z (2016) CO₂-induced phase engineering: protocol for enhanced photoelectrocatalytic performance of 2d MOS₂ nanosheets. *ACS Nano* 10:2903–2909
- [52] Jorgensen WL, Maxwell DS, Tirado-Rives J (1996) Development and testing of the OPLS all-atom force field on conformational energetics and properties of organic liquids. *J Am Chem Soc* 118:11225–11236
- [53] Hess B, Kutzner C, Van Der Spoel D, Lindahl E (2008) GROMACS 4: algorithms for highly efficient, load-balanced, and scalable molecular simulation. *J Chem Theor Comput* 4:435–447
- [54] Konatham D, Striolo A (2008) Molecular design of stable graphene nanosheets dispersions. *Nano Lett* 8:4630–4641
- [55] Span R, Wagner W (1996) A new equation of state for carbon dioxide covering the fluid region from the triple-point temperature to 1100 K at pressures up to 800 MPa. *J Phys Chem Ref Data* 25:1509–1596
- [56] Berendsen HJP, van Gunsteren WF, DiNola A (1984) J Haak Molecular dynamics with coupling to an external bath. *J Chem Phys* 81:3684–3690
- [57] Essmann U, Perera L, Berkowitz ML, Darden T, Lee H, Pedersen LG (1995) A smooth particle mesh Ewald method. *J Chem Phys* 103:8577–8593
- [58] Astrakas LG, Gousias C, Tzaphlidou M (2012) Structural destabilization of chignolin under the influence of oscillating electric fields. *J Appl Phys* 111:074702
- [59] Hess B, Bekker H, Berendsen HJ, Fraaije JG (1997) LINCS: a linear constraint solver for molecular simulations. *J Comput Chem* 18:1463–1472
- [60] Van Gunsteren WF, Berendsen HJ (1988) A leap-frog algorithm for stochastic dynamics. *Mol Simul* 1:173–185

Publisher's Note Springer Nature remains neutral with regard to jurisdictional claims in published maps and institutional affiliations.